

# Dependence of DNA Persistence Length on Ionic Strength of Solutions with Monovalent and Divalent Salts: A Joint Theory–Experiment Study

Annaël Brunet,<sup>†,‡,§</sup> Catherine Tardin,<sup>†,‡</sup> Laurence Salomé,<sup>†,‡</sup> Philippe Rousseau,<sup>||,⊥</sup> Nicolas Destainville,<sup>#,§</sup> and Manoel Manghi<sup>\*,#,§</sup>

<sup>†</sup>CNRS, Institut de Pharmacologie et de Biologie Structurale (IPBS) 205 route de Narbonne, BP 64182, F-31077 Toulouse, France

<sup>‡</sup>UPS, IPBS, Université de Toulouse F-31077 Toulouse, France

<sup>#</sup>UPS, Laboratoire de Physique Théorique (IRSAMC), Université de Toulouse, F-31062 Toulouse, France

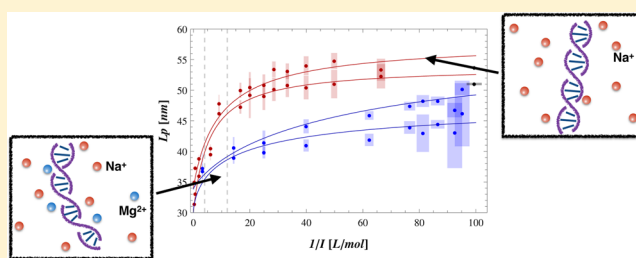
<sup>§</sup>CNRS, Laboratoire de Physique Théorique (IRSAMC), F-31062 Toulouse, France

<sup>||</sup>UPS, Laboratoire de Microbiologie et Génétique Moléculaires (LMGM), Université de Toulouse, F-31062 Toulouse, France

<sup>⊥</sup>CNRS, LMGM, UMR CNRS-UPS 5100, F-31062 Toulouse, France

## Supporting Information

**ABSTRACT:** Using high-throughput tethered particle motion single-molecule experiments, the double-stranded DNA persistence length,  $L_p$ , is measured in solutions with  $\text{Na}^+$  and  $\text{Mg}^{2+}$  ions of various ionic strengths,  $I$ . Several theoretical equations for  $L_p(I)$  are fitted to the experimental data, but no decisive theory is found which fits all the  $L_p$  values for the two ion valencies. Properly extracted from the particle trajectory using simulations,  $L_p$  varies from 30 to 55 nm, and is comparable to previous experimental results. For the  $\text{Na}^+$ -only case,  $L_p$  is an increasing concave function of  $I^{-1}$ , well fitted by Manning's electrostatic stretching approach, but not by classical Odjik–Skolnick–Fixman theories with or without counterion condensation. With added  $\text{Mg}^{2+}$  ions,  $L_p$  shows a marked decrease at low  $I$ , interpreted as an ion–ion correlation effect, with an almost linear law in  $I^{-1}$ , fitted by a proposed variational approach.



## 1. INTRODUCTION

Ions play a major role in the cell, for example, by modifying the protein activity, inducing a voltage between the intracellular and extracellular matrixes, or controlling the DNA packaging in viral capsids or in the nucleus. Complex mechanisms involving DNA, such as its wrapping around histones or its denaturation, will only be thoroughly understood when the effect of mobile ions on the DNA conformation is elucidated, DNA being one of the most charged biopolymers found in nature.

The first quantitative experimental studies of DNA conformational properties as a function of salt concentration were done in 1978 by Harrington,<sup>1</sup> using flow birefringence (FB) experiments, to measure the DNA radius of gyration in dilute DNA solutions. The DNA radius of gyration is intimately related to the DNA persistence length, namely the correlation length of the tangent–tangent correlation function,

$$\langle \mathbf{t}(s) \cdot \mathbf{t}(0) \rangle = \exp(-s/L_p) \quad (1)$$

where  $\mathbf{t}(s)$  is the unit vector tangent to the chain at the point of curvilinear index  $s$ . The persistence length,  $L_p$ , thus characterizes the chain stiffness at small length scales.

Experimentally, the persistence length has not been measured directly, and the required procedure to extract it

has remained a major issue since these first quantitative measurements.<sup>1</sup> Other optical techniques have been used, such as transient electric birefringence (TEB)<sup>2</sup> or magnetic birefringence (MB),<sup>6</sup> linear dichroism (LD),<sup>5</sup> dynamic light scattering (DLS),<sup>3</sup> and force-stretching by optical tweezers (FOT),<sup>7</sup> to estimate the variation of  $L_p$  as a function of the ionic strength  $I$ . In a recent paper, Savelyev<sup>4</sup> reviewed the available experimental data and showed that they could be divided into two groups based on the distinct behaviors of  $L_p$  found at high ionic strength. Indeed, whereas the first group of experimental data<sup>1,5–7</sup> indicated a slow decrease of  $L_p$  with increasing  $I$ , the second<sup>3,8–12</sup> found a significant decrease.

Hence, no global picture emerges yet from the literature. Many reasons can be put forward, such as the difficulty in estimating accurately the ionic strength in buffers, which is not simply equal to the added salt concentration, or the method of extraction of the persistence length from the experimental observables. Indeed, extraction of the variations of  $L_p$  with  $I$  by using FB, MB, and LD techniques is very sensitive to the

Received: April 9, 2015

Revised: May 19, 2015

Published: May 29, 2015

optical arrangement between the electric field and the molecular axis, which is related to the tedious evaluation of the magnetic/optical anisotropy of a single base-pair (bp). Moreover, in LD experiments, the mechanism of interaction between nucleic acids and the electric field depends on the polarizability of the ionic cloud surrounding the DNA, which therefore requires an additional modeling. In FOT experiments, the high DNA stretching induced by the force modifies the DNA structure and the organization of its ionic cloud. Finally, in DLS experiments, the DNA hydrodynamic radius is estimated from the measured diffusion coefficient. Inferring the persistence length is not easy, especially due to excluded volume effects.

Among the different theories developed to explain the variations of  $L_p$  with the ionic strength,  $I$ , the most famous is the Odjik–Skolnick–Fixman (OSF) theory,<sup>13,14</sup> where  $L_p$  is the sum of a bare, non-electrostatic persistence length and an electrostatic contribution scaling as  $I^{-1}$ . This theory accounts, at least qualitatively, for the fact that a rise in  $I$  provokes an increasing screening of the repulsive phosphate ions of the backbone, which leads to a more flexible DNA chain. Taking into account the so-called Manning counterion condensation around the DNA at low  $I$ , the prefactor in front of  $I^{-1}$ , proportional to the square of the effective DNA charge, is lowered. All the experimental works have therefore been compared to these types of theoretical approaches, with no decisive conclusion.<sup>4</sup> More recently, Manning proposed a new theory,<sup>15</sup> explicitly considering the electrostatic stretching force of the polyelectrolyte, which qualitatively fits some experiments<sup>7</sup> or numerical results at high  $I$ .<sup>4,16</sup>

In this paper we reconsider the old issue, still under debate,<sup>17</sup> of the dependence of DNA conformation, at room temperature, on the ionic strength of the surrounding solution, using the recent single-molecule technique of high-throughput tethered particle motion (HT-TPM).<sup>18,19</sup> We measure the persistence length of two DNAs, of 1201 and 2060 bps, for a large range of well-controlled ionic strengths from  $I = 10^{-2}$  to 3 mol/L with  $\text{Na}^+$  counterions and with or without added  $\text{Mg}^{2+}$  counterions. We assume that the tangent–tangent correlation function is well described by a single persistence length,  $L_p$ , following eq 1. In section 2, we present the simple and well-controlled HT-TPM experiments and their analysis. Section 3 is devoted to the experimental results and the extraction of the persistence length from the HT-TPM amplitude of motion using numerical simulations. Our results are then compared to previous ones in section 4, and to the various existing theories as well as our detailed variational approach in section 5. An interpolation formula that fits all our experimental  $L_p$  values is presented in section 6. Finally, our concluding remarks are given in section 7.

## 2. EXPERIMENTAL SECTION

**2.1. High-Throughput Tethered Particle Motion Experimental Procedure.** DNA molecules were produced by polymerase chain reaction amplification (oligonucleotides from Sigma-Aldrich): Biot-F1201 5'-CTGGTGAGTACTCAACCAAG-3' and Dig-R1201 5'-CTACAATCCATGCCAACC-3' on pTOC1 plasmid, and Biot-F2060 5'-CTGCAATGATACCGCGAGAC-3' and Dig-R2060 5'-TGAC-TTCCGCGTTTCCAGAC-3' on pBR322.

HT-TPM permits the simultaneous tracking of hundreds of single DNA molecules free to fluctuate in solution that are tethered to a coverslip at one end and labeled by a 300 nm particle at the other end (see Figure 1). HT-TPM on-chip assembly is performed as previously described in detail in ref 19. Anchoring of the DNA–particle

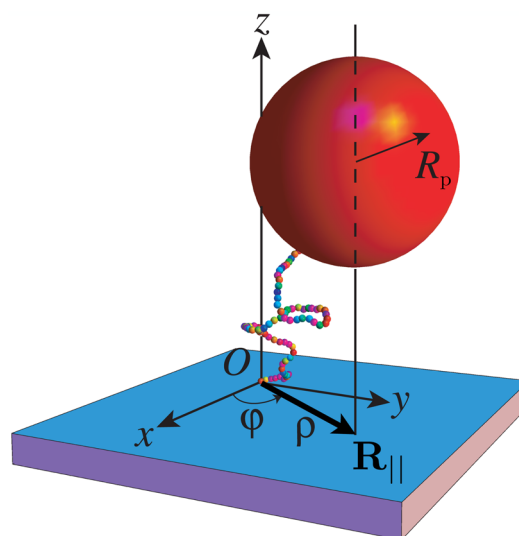


**Figure 1.** Principle of the tethered particle motion experiment. The DNA is tethered at one end on the coverslip and labeled by a particle (radius  $R_p$ ) at the other end. The projected particle position  $R_{||}$  is tracked as a function of time. The DNA is modeled by a chain of beads in the simulations.

complexes to the neutravidin (Invitrogen) printed sites was performed in phosphate-buffered saline (Euromedex) supplemented with 1 mg/mL of pluronic 127 (Sigma-Aldrich) and 0.1 mg/mL bovine serum albumin (Sigma-Aldrich), noted T-BSA-Plu.

A large range of buffers were then used to test the effects of both ion valency, by using monovalent  $\text{Na}^+$  or divalent  $\text{Mg}^{2+}$ , and salt concentration on the DNA conformations (Tables I and II in the Supporting Information). The first buffer, corresponding to zero salt added and called zero-salt-buffer in the following, is a phosphate buffer ( $\text{KH}_2\text{PO}_4$  1 mM,  $\text{Na}_2\text{HPO}_4$  3 mM, pH 7.4, pluronic F127 1 mg/mL). To this, we added successively various concentrations of  $\text{NaCl}$  or  $\text{MgCl}_2$  to obtain a large range of salt conditions (X-salt-buffer). Before starting the experiment, the flow cell was extensively rinsed with the zero-salt-buffer ( $\sim 100$  chamber volumes), left to incubate for 1 h at room temperature, and then rinsed again with  $\sim 100$  chamber volumes of zero-salt-buffer. The experiment started with a zero-salt-buffer measurement; next, the concentration of monovalent ions was progressively increased by addition of  $\sim 100$  chamber volumes of X-salt-buffer. The flow cell was extensively rinsed with the zero-salt-buffer ( $\sim 100$  chamber volumes), incubated for 4 min, and rinsed again with  $\sim 100$  chamber volumes of zero-salt-buffer. A new zero-salt-buffer measurement was performed. At last, the divalent ion concentration was progressively increased, and new measurements were carried out. For all conditions, the data acquisition was performed at a controlled temperature of 25 °C, and 1 min movie was recorded and analyzed. We ensure the reliability of the experimental procedure by checking the agreement between the two values of the zero-salt measurement obtained before the addition of monovalent ions and before the addition of divalent ions. Experiments were repeated on different days to ensure the reproducibility of our results.

The tethered particles of 300 nm diameter were visualized using a dark-field microscope (Axiovert 200, Zeiss) equipped with a 32 $\times$  objective, an additional 1.6 $\times$  magnification lens, and a temperature control system (Physitemp TS-4MPER). Images were acquired during 1 min at a frame recording rate of 25 Hz on a Dalsa Falcon 1.4M100 CMOS camera. The field of observation covers an area of 215  $\mu\text{m} \times 160 \mu\text{m}$ .

**2.2. HT-TPM Procedure of Analysis.** The software developed by Magellium (France) tracks in real time the positions of all the particles, corrects for experimental drift, calculates the asymmetry factor to select tethered particles valid for the analysis, and finally projects the experimental root-mean-square end-to-end distance on the surface,  $R_{\text{exp}||} \equiv \sqrt{\langle R_{||}^2 \rangle}$ , the amplitude of motion of the bead, along the time

trace (see Figure 1). We refer the reader to ref 21 for the detailed calculations of  $R_{\text{exp}\parallel}$ .

In order to measure the small differences expected on  $R_{\text{exp}\parallel}$ , we set up a two-step procedure for the analysis of  $R_{\text{exp}\parallel}$  where first a criterion of validity and then some corrections are applied. This procedure was performed with home-built Mathematica scripts. Details can be found in ref 19. During this procedure, around 12% of the data was eliminated, and the final number of trajectories kept for each DNA condition typically ranged between 100 and 1000 (see Tables I and II in the Supporting Information).

### 3. EXPERIMENTAL RESULTS

#### 3.1. Simple Estimate of DNA Persistence Length from the Amplitude of Motion.

In Figure 2 are shown the

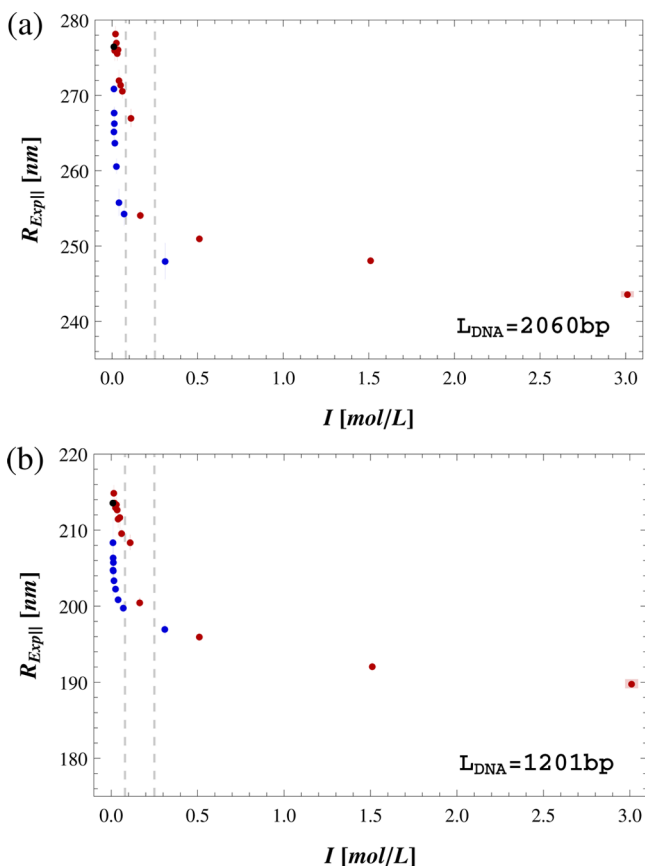


**Figure 2.** Experimental HT-TPM amplitude of motion vs the ionic strength  $I$  for a DNA of length (a)  $L = 2060$  bp and (b)  $L = 1201$  bp with  $\text{Na}^+$  (red) and  $\text{Mg}^{2+}$  (blue) cations. Vertical lines delimit the close-to-physiological salt conditions, as listed in Table 1.

variations of the experimental amplitude of motion, i.e., the root-mean-square end-to-end distance projected on the surface,  $R_{\text{exp}\parallel}$ , measured by HT-TPM, as a function of the ionic strength,  $I$ , of the various buffers listed in Tables I and II in the Supporting Information for two DNA of lengths 2060 and 1201 bp. The ionic strength is defined as

$$I = \frac{1}{2} \sum_i z_i^2 c_i \quad (2)$$

where  $z_i$  and  $c_i$  are respectively the valency and the concentration of ion  $i$  in the buffer. The red (resp. blue) symbols correspond to the monovalent  $\text{Na}^+$  ions (resp. divalent  $\text{Mg}^{2+}$  ions) added to the buffers. The black symbols correspond to zero-salt-buffer conditions.

The plots clearly show that, when  $I$  is increased,  $R_{\text{exp}\parallel}$  decreases by about 10% for monovalent as well as divalent ions. This is thus a subtle effect. This behavior is qualitatively due to the fact that negatively charges carried all along the DNA repel each other more strongly when the ionic strength is low; this repulsion decreases when the ionic strength increases due to electrostatic screening. This self-repulsion increases the rigidity of the macromolecule, thus increasing  $R_{\text{exp}\parallel}$ . Furthermore, one notices that the variation of  $R_{\text{exp}\parallel}$  is amplified when the DNA length,  $L$ , is increased. This is consistent with the fact that the process under examination occurs homogeneously along the DNA.

Comparing the experimental results for monovalent and divalent ions over the same  $I$  range, one observes that the decrease of  $R_{\text{exp}\parallel}(I)$  is more important with  $\text{Mg}^{2+}$  ions, and once again the effect is amplified for long DNAs. Moreover, one notes a sudden drop of  $R_{\text{exp}\parallel}$  at very low concentrations of  $\text{Mg}^{2+}$  (from  $I = 10.1$  mmol/L without  $\text{Mg}^{2+}$  to 10.5 mmol/L). However, it is difficult to know with high precision the ionic strength for such low values, since we cannot exclude that some additional ions are released from the surface, for instance. Therefore, the errors bars are potentially large for these points.

To access the properties of the DNA only, such as its end-to-end distance,  $R_{\text{DNA}} \equiv \sqrt{\langle R_{\text{DNA}}^2 \rangle}$ , it is necessary to correct for the effects of the particle and the glass substrate. The simplest way is to subtract the particle radius by assuming that the DNA extremity and the particle, of radius  $R_p = 150$  nm, move independently, which leads to<sup>19</sup>

$$\langle R_{\text{DNA}}^2 \rangle = \frac{3}{2} \langle R_{\parallel}^2 \rangle - R_p^2 \quad (3)$$

By doing so, we neglect the effect of the glass substrate. It has been taken into account analytically only for long and flexible polymers,<sup>23</sup> which is not the case for the DNA in this study. Indeed, their length ( $L = 2060$  and 1201 bp, i.e., 700 and 408 nm, using 1 bp = 0.34 nm) is no more than a few persistence lengths ( $L_p \approx 50$  nm), which allows us to qualify them as semiflexible. As already shown in ref 19, the approach proposed in ref 23 does not work well for such DNA lengths. [The approach proposed in ref 23 yields essentially the same result as eq 3 for  $N = 2060$  and is not valid for  $N = 1201$ .]

Figure 1 in the Supporting Information shows the DNA end-to-end distance,  $R_{\text{DNA}}$ , obtained by eq 3, as a function of the inverse of the ionic strength,  $I^{-1}$ . Of course, the relative effect of the salt is slightly higher once the particle radius is deduced. The next step is to extract the DNA persistence length,  $L_p$ , from  $R_{\text{DNA}}$ . The simplest way would be to use the wormlike chain (WLC) formula, valid for a phantom chain in solution, resulting from eq 1:<sup>24</sup>

$$\langle R_{\text{DNA}}^2 \rangle = 2L_p^2 \left( \frac{L}{L_p} - 1 + e^{-L/L_p} \right) \quad (4)$$

However, this way of extracting  $L_p$  leads to quite high values of the persistence length compared to the commonly accepted values around 50 nm. For instance, at low  $I$ ,  $L_p$  saturates around 76 nm for the 2060 bp long DNA and around 68 nm for the 1201 bp long DNA (data not shown). These high values might be due to the particle–substrate interaction, or particle–polymer or monomer–monomer excluded volume interactions, which may swell the DNA.

**3.2. Refined Extraction of the DNA Persistence Length Using Simulations of the HT-TPM Setup.** To check these

effects and the approximations used in eqs 3 and 4, we performed numerical simulations. DNA–particle conformations are computed numerically by exact sampling.<sup>23</sup> The labeled DNA polymer is generated as a random walk of  $N$  steps, corresponding to the links of length  $2a$ , with a bending energy by step,  $E_{\text{bend}} = -\kappa_b \cos \theta$ , where  $\kappa_b$  is the bending modulus and  $\theta$  is the angle between successive steps. The number of steps  $N$  was chosen such that  $a = 6$  bp, corresponding to the DNA diameter. The starting point is on the substrate, and at each step, self-intersecting trajectories (resp. trajectories intersecting the substrate) are eliminated to take into account intrachain excluded volume interactions (resp. repulsive interactions with the substrate). Hence, the polymer is modeled by a chain of beads of (excluded) volume  $v = 4\pi a^3/3 \simeq 36$  nm<sup>3</sup>, which is taken to be constant as a function of the ionic strength (see Figure 1). The salt effects are therefore supposed to be completely taken into account in the bending modulus,  $\kappa_b$ . The last step, of length  $a + R_p$ , has a uniformly random orientation. The persistence length value is related to  $\kappa_b$  by  $L_p = 2a\beta\kappa_b$ , where  $\beta = (k_B T)^{-1}$  is the inverse of the thermal energy. [Strictly speaking, the discrete WLC persistence length leads to  $L_p = -2a/\ln[\coth(\beta\kappa_b) - 1/\beta\kappa_b]$ . For  $L_p \in [35, 70]$  nm, the error is less than 0.25 nm when using the approximation  $L_p \simeq 2a\beta\kappa_b$ .] The two-dimensional projection of the particle position,  $\mathbf{R}_{\parallel}$ , was measured, and the amplitude of motion, defined as  $R_{\parallel} \equiv \sqrt{\langle \mathbf{R}_{\parallel}^2 \rangle}$ , is averaged over several million independent trajectories. Since at this level of coarse-graining, electrostatic interactions are not included, we varied  $\kappa_b$  by hand such that  $L_p$  spans the range 36–70 nm, in order to reflect the stiffening due to the decrease of the ionic strength in the solution. We do not consider the torsional degrees of freedom in these simulations, since no constant torque is applied on the particle and therefore on the DNA. Hence, the end-to-end distance (eq 4), the quantity of interest here, is not modified by torsional fluctuations as soon as, at this level of coarse-graining, the DNA is locally viewed as a straight cylinder (model KP1 as defined in ref 25).

Figure 3 shows the simulated  $R_{\parallel}$  as a function of  $L_p$  (full circles). We observe an increase of  $R_{\parallel}$  from 240 to 300 nm for the 2060 bp long DNA, and from 195 to 230 nm for the 1201 bp long DNA. Both ranges of  $R_{\parallel}$  values contain the corresponding experimental observations, which thus indicates that we explored a good range of persistence length values.

For the purpose of comparison, we also plotted the end-to-end distance of a free polymer–particle complex without any excluded volume interactions and without wall (triangles), and the polymer–particle plus substrate without excluded volume (open circles). The solid curves correspond to the discrete WLC result for the end-to-end distance, using eq 3 (to include the particle contribution), and without any excluded volume and wall:<sup>26</sup>

$$\langle \mathbf{R}_{\parallel}^2 \rangle = \frac{2}{3} [a^2 N W_N(v(\kappa_b)) + R_p^2] \quad (5)$$

where

$$W_N(x) = \frac{1+x}{1-x} - \frac{2x}{N} \frac{1-x^N}{(1-x)^2} \quad (6)$$

and  $v(\kappa_b) = \coth(\kappa_b) - 1/\kappa_b$ . Clearly, the solid curve perfectly matches the simulation results, as expected. The dashed line corresponds to the continuous WLC (no excluded volume and no wall), eq 4, which gives slightly larger end-to-end distances.

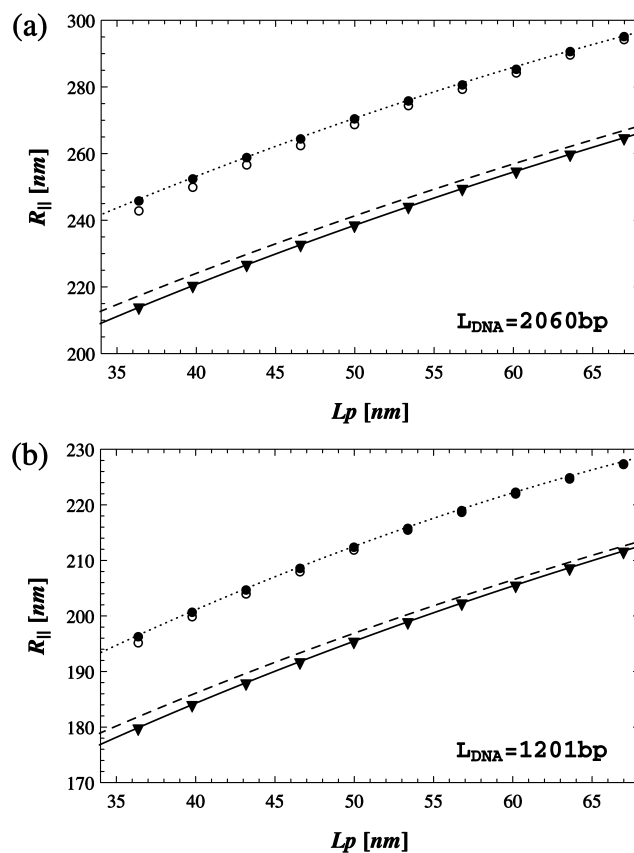


**Figure 3.** Simulated  $R_{\parallel}$  vs  $L_p$  for DNA of (a) 2060 bp ( $N = 172$ ) and (b) 1201 bp ( $N = 100$ ). Triangles correspond to a free polymer–particle complex without excluded volume. Full (resp. open) circles correspond to a grafted polymer in the TPM geometry with a hard core particle and with (resp. without) intrachain excluded volume interactions (see text). The solid line is the discrete WLC formula, eq 5; the dashed line is the continuous WLC formula, eq 4; and the dotted lines are fits by polynomials: (a)  $R_{\parallel} = (-10.7 \times 10^{-3})L_p^2 + 2.71L_p + 162.1$  [nm], and (b)  $R_{\parallel} = (-9.0 \times 10^{-3})L_p^2 + 1.955L_p + 137.35$  [nm].

One observes that the presence of the particle that interacts with both the substrate and the chain induces a non-constant shift to higher values of  $R_{\parallel}$  (from triangles to full circles). Since the intrachain excluded volume swells the polymer by less than 2 nm, especially for small values of  $L_p$  (more flexible chains), the main difference comes from the substrate–particle interactions. This is why the extraction of  $L_p$  using eqs 3 and 4, or equivalently eq 5, overestimates  $L_p$  by about 20 nm.

To obtain precise values of  $L_p$  from the experiments, we thus fitted the simulation data  $R_{\parallel}(L_p)$  by a quadratic polynomial law (see Figure 3), which in turn allows us to accurately determine the experimental  $L_p$  from the experimental values of  $R_{\parallel}$ . The persistence length is then plotted as a function of  $I^{-1}$  in Figure 4 for the two DNA lengths and the two types of counterions (figures are given in Tables I and II in the Supporting Information). Other available data found in the literature are also shown.

With Na<sup>+</sup> counterions,  $L_p$  values are in the same range for both  $L = 2060$  and 1201 bp, which tends to confirm that the persistence length extracted with this procedure is almost independent of the DNA length, as expected. It increases monotonically from roughly 35 nm for high ionic strength ( $I \simeq 3$  mol/L) to 54 nm for low ionic strength ( $I = 10$  mmol/L),

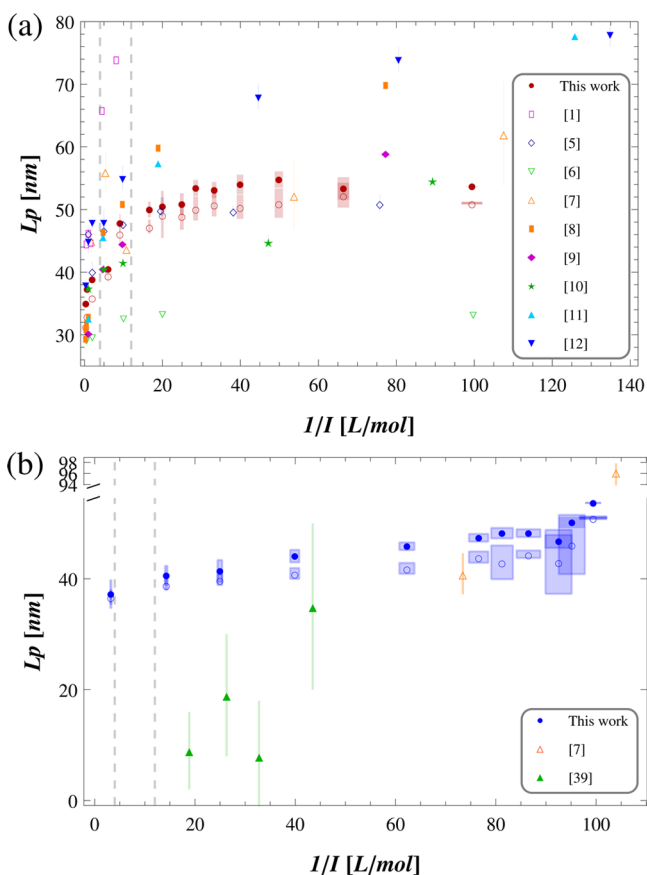


**Figure 4.** DNA persistence length,  $L_p$ , vs the inverse of the ionic strength,  $I^{-1}$ , extracted from the HT-TPM data (full circles for  $L = 2060$  bp and open circles for  $L = 1201$  bp), and from available literature data (references are given in the legend). Buffers with (a) monovalent  $\text{Na}^+$  salt counterions and (b) added divalent  $\text{Mg}^{2+}$  counterions.

which corresponds to an increase of more than 50%. Near physiological salt conditions, around 150 mmol/L, we find  $L_p \approx 43$  nm. Moreover, using this plot representation, the data show a clear concave shape.

With  $\text{Mg}^{2+}$  counterions,  $L_p$  is greatly reduced, which is a signature of the role of the ion valency  $z$ . This has already been observed in previous experiments.<sup>2,7</sup> The  $L_p$  values, between 35 and 50 nm, are slightly different for the two DNAs,  $L_p$  being larger by almost 5 nm at low  $I$  for the longest DNA. Moreover, we observe an abrupt decrease of  $L_p$  between the case of no divalent ions and the previous  $I^{-1}$  value, corresponding to the addition of 0.15 mmol/L of  $\text{Mg}^{2+}$ . At higher  $I$ , the increase of  $L_p$  is almost linear in  $I^{-1}$ .

In the following, we shall try to fit the so-obtained DNA persistence lengths using the available theories found in the literature. Before this, we compare our experimental values to the ones found in the literature.

#### 4. COMPARISON WITH OTHER EXPERIMENTAL DATA

**4.1. Influence of  $\text{Na}^+$  Monovalent Ions.** We start the comparison with other experimental studies by focusing on the measurements of  $L_p$  for values of  $I$  close to the physiological salt conditions. The behavior of  $L_p$  under the action of ionic strength is then discussed.

*Persistence Length Close to the Physiological Salt Concentration.* An inventory of the values of  $L_p$  measured

near physiological salt conditions, i.e., for  $I \in [100, 200]$  mmol/L with only monovalent  $\text{Na}^+$  counterions, is presented in Table 1. The mean value of these  $L_p$  values found in refs 5, 7–12, and

**Table 1. Summary of  $L_p$  Measured in the Close-to-Physiological Salt Conditions (with  $\text{Na}^+$ ) Found in the Literature<sup>a</sup>**

$I$ [mmol/L]	$L_p$ [nm]	$L_{\text{DNA}}$ [bp]	experimental method	ref
223.0	$66 \pm 3$	6646	FB (25 °C)	1
210.8	46.5	6646	DLS (20 °C)	8
210.8	54.7	6646	DLS (20 °C)	11
210.8	40.6	6646	DLS (20 °C)	9
204.1	$48 \pm 2$	39936	DLS (20 °C)	12
201.0	$40.6 \pm 0.4$	39936	FB (25 °C)	10
201.0	$46.8 \pm 0.4$	39936	LD	5
186.2	$56 \pm 3$	48502	FOT (25 °C)	7
165.1	$40.5 \pm 0.4$	2060	HT-TPM (25 °C)	this work
165.1	$39.5 \pm 0.5$	1201	HT-TPM (25 °C)	this work
154.0	$50 \pm 5$	434, 587	TEB (20 °C)	2
123.0	$74 \pm 3$	6646	FB (25 °C)	1
110.1	$47.8 \pm 0.7$	2060	HT-TPM (25 °C)	this work
110.1	$46.2 \pm 0.8$	1201	HT-TPM (25 °C)	this work
103.1	44.6	6646	DLS (20 °C)	8
103.1	44.6	6646	DLS (20 °C)	9
103.1	$53 \pm 2$	39936	DLS (20 °C)	12
102.4	$55 \pm 2$	39936	DLS (20 °C)	12
101.1	$43 \pm 1$	43–179	TED (20 °C)	28
101.0	$47.8 \pm 0.4$	39936	LD	5
101.0	$41.8 \pm 0.6$	39936	FB (25 °C)	10
93.4	$43 \pm 1$	48502	FOT (25 °C)	7

<sup>a</sup>In order to compare the whole set of published data,<sup>5,7–12,28</sup> we rigorously computed the ionic strength used in these data by directly taking experimental values when available, or the values deduced by interpolation otherwise.

28 is  $48 \pm 6$  nm, which is in good agreement with our interpolated value:  $L_p(150 \text{ mmol/L}) = 43 \pm 3$  nm. In fact, the measured  $L_p$  varies widely with the experimental techniques used, with the studied DNA (with lengths varying from 6646 bp to 50 kbp), and with the theoretical and analytical tools used to extract  $L_p$ . In addition, the variability of these  $L_p$  values might be attributed to the difficulty in perfectly controlling the presence of divalent ions such as  $\text{Mg}^{2+}$ , the presence of which can have a dramatic effect even at low concentrations (on the order of mmol/L), as mentioned before. Finally, it can be noted that the commonly accepted value of  $L_p = 50$  nm for a “random” DNA sequence at physiological salt conditions, i.e.,  $I \approx 150$  mmol/L ( $I^{-1} \approx 6.7$  L/mol) with only monovalent  $\text{Na}^+$  counterions,<sup>27</sup> slightly exceeds the experimentally derived values.

*Variation of  $L_p$  on the Whole  $I$  Range.* In order to compare the global behavior of  $L_p(I)$  that we measured with the previously published results, we superimposed all the results in Figure 4a, where  $L_p$  values are plotted as a function of  $I^{-1}$ . As mentioned in the Introduction, Savelyev<sup>4</sup> recently reviewed all the available experimental data and showed that they could be divided into two groups, based on the difference in  $L_p$  behaviors observed at high ionic strength,  $0.11 \leq I \leq 3$  mol/L (see Figure 4). We will keep this division to compare our results to those obtained from the first group of experimental data,<sup>1,5–7</sup> which shows a slow decrease of  $L_p$  with increasing  $I$ , and then to those

obtained from the second group of data,<sup>3,8–12</sup> which found a significant decrease of  $L_p$ .

In the first set of experiments, the researchers observed a saturation of  $L_p$  at high  $I$ . More precisely, for  $I$  exceeding 150 mmol/L,  $L_p$  decreased by only 10%. Moreover, at low  $I$ , these publications showed an increase in  $L_p$  of about 10%, similar to our observations from our HT-TPM measurements. It can be noted that Harrington<sup>1</sup> found a larger increase of  $L_p$  in the low  $I$  range than all the other results.

This first group of experimental works gathers results obtained by FB from Harrington,<sup>1</sup> MB from Maret et al.,<sup>6</sup> FOT from Baumann et al.,<sup>7</sup> and LD from Rizzo et al.<sup>5</sup> [We recalculated the  $L_p$  values (between 30 and 90 nm) reported Maret et al. by using the raw data collected in Table 1 and eq (5) of ref 6. Our calculation does not correspond to the data reported by Savelyev et al.<sup>4,16</sup>] The FB, MB, or LD methods may be prone to perturbative Joule heating and bulk electrophoresis effects; to minimize these effects, the ionic strength was kept low. As the FOT method induces a perturbation of the sample structure in the high force regime, we consider only the  $L_p$  values obtained in the low force regime, using the inextensible WLC model as a comparison to our HT-TPM results, where no force is applied. It is important to note that these studies were performed on DNA exceeding 40 kbp long, and that only scarce measurements were performed at high ionic strength, in opposition to the second group of data.

In this regime of high ionic strength, the second group did not show a plateau but rather a significant decrease of  $L_p$  by about 25–30%. This observation is in good agreement with our measured decrease of 25% in the same  $I$  range. In the low ionic strength range,  $0.01 \leq I \leq 0.1$  L/mol, this second group measures a small but regular decrease of  $L_p$  by about 15% when  $I$  increases, which is larger than the decrease we measured, about 10%. FB data<sup>10</sup> can be classified in this set of data, given the 25% increase of  $L_p$  in the high  $I$  range. However, variations in the low ionic strength range seem to be modest in comparison to the other publications of this set, but closer to ours.

This second group of experimental data is essentially based on the DLS experiments performed by Sobel et al.<sup>12</sup> and Kam et al.<sup>9</sup> Manning<sup>8</sup> and Post<sup>11</sup> proposed corrections to the extracted  $L_p$  values from the original data reported by Borochoy et al.<sup>3</sup> In those DLS experiments, the DNA hydrodynamic radius was deduced from the diffusion coefficient measurement. To infer  $L_p$ , the usual Gaussian polymer model was used. The number of Kuhn segments being large for the 6646 bp (resp. ~40 kbp) DNA under study,  $N \simeq 22$  (resp.  $N \simeq 1333$ ), the swelling of the chain was induced as a result of excluded volume. Therefore, it is essential to precisely estimate the excluded volume. This is nevertheless a challenging task. For instance, Manning's<sup>8</sup> and Post's<sup>11</sup> corrections led to  $L_p$  values differing by 4 nm at  $I = 8$  mmol/L and by ~1 nm at  $I = 1$  mol/L.

Note that we compare studies performed on long DNA, from 6646 bp to 40 kbp, which are in the flexible regime and thus much more sensitive to excluded volume effects than our HT-TPM experiments made on DNA of lengths  $L = 2060$  or 1201 bp, which are in the semiflexible regime.

In this quantitative comparison, we only considered experiments performed on the same range of ionic strength induced by  $\text{Na}^+$  ions. As a result, refs 2 and 27–34, which studied the effect of very low  $\text{Na}^+$ -induced  $I$ , as well as refs 35

and 36, which focused on the influence of  $\text{K}^+$  or  $\text{Li}^+$  ions, and ref 37, which studied the combined effect of multivalent and monovalent ions, were discarded from our comparison. Note that the single-molecule study in ref 38 was not considered either because too few values of  $I$  were explored.

**4.2. Influence of  $\text{Mg}^{2+}$  Divalent Ions.** The decrease of  $L_p$  that is measured when  $I$  is varied from 10 to 310 mmol/L is about 35% whatever the ion valency and the DNA length (Figure 4). Yet the shape of this decrease as a function of  $I$  is completely different, depending on the valency of the ions used. Divalent ions appears to induce an almost linear decrease of  $L_p$  as a function of  $I^{-1}$ , while monovalent ions cause a decrease with a concave shape. In addition, the absolute value for  $L_p$  is smaller by about 5 nm with divalent ions than with monovalent ions at low  $I$ . This observed trend is in agreement with the first quantitative observations at very low  $I$  by Hagerman,<sup>2</sup> Elias and Eden,<sup>29</sup> and then others.<sup>6,7</sup> In addition, Hagerman<sup>2</sup> observed on 434 and 587 bp DNA by TEB the same abrupt decrease of  $L_p$  at very low  $I$  with  $\text{Mg}^{2+}$  ions, followed by a slower decrease, as shown in Figure 7. The magnitude of this initial decrease was, however, larger by around 30% in ref 2, and 60% in ref 7, whereas ref 6 found a decrease similar to ours.

Some other studies explored the influence of  $\text{Mg}^{2+}$  on DNA flexibility<sup>28,32,34,36,40,41</sup> and showed a rise in DNA flexibility with the addition of  $\text{Mg}^{2+}$  counterions in solution. Nevertheless, these studies probed only a few values of  $I$ , and some KCl was added to the solution, preventing any quantitative comparison.

Dietrich et al.<sup>39</sup> also used the TPM technique to monitor the effect of  $\text{Mg}^{2+}$  on a DNA fragment of 4882 bp and observed a large decrease of  $R_{\text{exp}\parallel}$  in the presence of divalent ions. Yet the  $L_p$  values extracted from these experimental data, much smaller than any other published experimental data, cannot be quantitatively compared to our results due to several errors in the extraction procedure. The persistence length was extracted assuming that the particle excursion was related to  $L$  using a simple Hooke law in the Gaussian regime,  $\langle R^2_{\parallel} \rangle = 2L_p L$ , thus seemingly forgetting the factor 3/2 due to dimensionality and not subtracting the particle radius (see eq 3), but also ignoring excluded volume effects. Moreover, they presented a very large error bar of 10 nm, due to the small number of trajectories, ranging between 6 and 27.

In the next section, we compare our experimental values of the DNA persistence length to the various theories developed in the literature.

## 5. COMPARISON BETWEEN EXPERIMENTS AND EXISTING THEORIES

**5.1. Odijk–Skolnick–Fixman Approach at High Ionic Strength.** Several models have been proposed in the literature to explain the variation of the persistence length,  $L_p$ , of polyelectrolytes with the ionic strength,  $I$ . When electrostatic interactions between mobile ions and the polyelectrolyte are taken into account at the Debye–Hückel level (mean-field level and approximation of small values of the electrostatic potential), it has been shown by Odijk<sup>13</sup> and Skolnick and Fixman<sup>14</sup> (OSF) that, using a perturbative approach around an infinitely stiff rod, the persistence length has two contributions,

$$L_p^{\text{OSF}} = L_p^{\infty} + \frac{l_B}{4A^2\kappa^2} \quad (7)$$

where  $L_p^\infty$  is the bare persistence length (in the limit  $\kappa A \rightarrow \infty$ ), and the second term is an electrostatic contribution to  $L_p$ , where  $A$  is the distance between elementary charges along the chain and

$$\kappa = \sqrt{8\pi l_B I} \quad (8)$$

is the Debye–Hückel screening parameter. The Bjerrum length,  $l_B = e^2/4\pi\epsilon k_B T$ , is equal to 0.715 nm in water at room temperature, which yields  $\kappa = 3.29\sqrt{I} \text{ nm}^{-1}$  (where  $I$  is in mol/L). Equation 7 is theoretically valid for polymer conformations close to the rodlike one, i.e., for  $l_B L_p^\infty \gg A^2$ .

For a dsDNA, with two phosphate anions per bp, we have  $A = 0.17 \text{ nm}$  and  $L_p^\infty \approx 50 \text{ nm}$ , so the validity of eq 7 is well verified. As a function of the ionic strength,  $I$ , eq 7 can be rewritten as

$$L_p^{\text{OSF}} = L_p^\infty + \frac{0.559}{I} [\text{nm}] \quad (9)$$

where  $I$  is in mol/L. Note that the numerical value of the coefficient depends on the model, as shown by Fixman.<sup>42</sup> In any case, Fixman affirms that the exponent in  $I^{-1}$  is robust at large  $I$  (large  $\kappa$ ). Clearly the data in Figure 5, where the

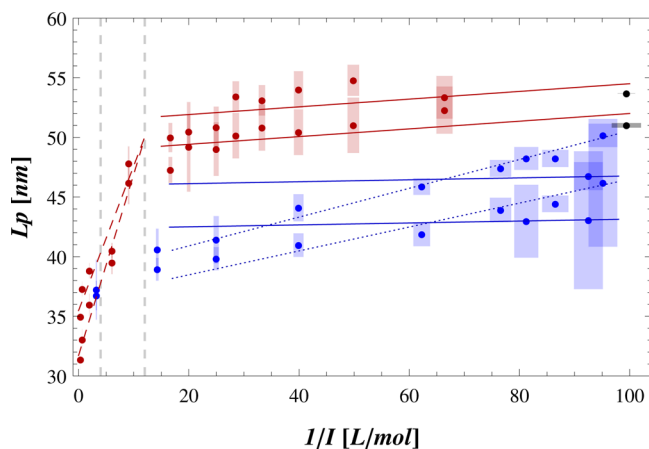


**Figure 5.** Linear fits of the persistence length,  $L_p$ , measured by HT-TPM (already shown in Figure 4) vs the inverse of the ionic strength,  $I^{-1}$ . Dashed lines correspond to eq 7 for large  $I^{-1}$ ,  $L_p^\infty + C/I$ , with two fitting parameters (see text for values), and solid lines to eq 11 for low  $I^{-1}$ , with  $L_p^0$  as fitting parameter. Better fits are obtained for  $\text{Mg}^{2+}$  by leaving  $B$  free (dotted lines,  $L_p^0 = 38.5 \text{ nm}$ ,  $B = 0.121$  for  $L = 2060 \text{ bp}$ , and  $L_p^0 = 36.5 \text{ nm}$ ,  $B = 0.1$  for  $L = 1201 \text{ bp}$ ).

experimental  $L_p$  is plotted vs  $I^{-1}$ , show a concave shape for high ionic strength, and therefore are not well fitted by the linear law, eq 9. Figure 5 shows a linear fit (dashed lines),  $L_p^\infty + C/I$ , for  $0 < I^{-1} < 10 \text{ L/mol}$ , which yields  $C = 1.21 \text{ nm}\cdot\text{mol/L}$  and  $L_p^\infty = 35.5 \text{ nm}$  for  $L = 2060 \text{ bp}$ , and  $C = 1.52 \text{ nm}\cdot\text{mol/L}$  and  $L_p^\infty = 31.7 \text{ nm}$  for  $L = 1201 \text{ bp}$ , which are almost 3 times larger than the values predicted by OSF. Since we do not have enough data at very high  $I$  with added  $\text{Mg}^{2+}$ , we did not try to fit eq 9 for the  $\text{Mg}^{2+}$  case.

The data obtained by the first group<sup>1,5–7</sup> at high  $I$  were qualitatively in agreement with the OSF theory, in the sense that the variations of  $L_p$  are small at high  $I$ . However, no fit using eq 7 was done in those works.

**5.2. Manning Charge Renormalization at Low Ionic Strength.** The OSF theory fails to explain the variation of  $L_p(I^{-1})$  for the whole range of  $I$  studied; indeed, it does not

reproduce the concave shape observed in Figure 7. A plausible explanation is that the Debye–Hückel approximation of small values of the electrostatic potential is not valid for double-stranded (ds) DNA, which is highly charged. Indeed, Manning showed in the 1960s that, in the limit of low  $I$ , some counterions somehow “condense” close to the DNA due to the large net charge of DNA.<sup>43</sup> This effect is a nonlinear effect associated with the mean-field Poisson–Boltzmann equation close to charged cylinders. This phenomenon, known as the Manning condensation, tends to reduce the effective charge of the DNA. Manning proposed that, in the *low salt limit*, the effective linear charge density is  $\alpha/A$ , where  $\alpha$  depends on the parameter

$$u = \frac{z l_B}{A} \quad (10)$$

where  $z$  is the counterion valency. If  $u < 1$ ,  $\alpha = 1$ , and if  $u > 1$  then  $\alpha = 1/u$ . For dsDNA, the Manning parameter is  $u = 4.21$  for  $\text{Na}^+$  counterions ( $z = 1$ ) and  $u = 8.41$  for  $\text{Mg}^{2+}$  ( $z = 2$ ). Thus, for monovalent counterions,  $\alpha = 0.24$ , and the effective charge is decreased by a factor of roughly 75%. For a mixture of counterions with different valencies, which is the case in our experiments with  $\text{Mg}^{2+}$  ions, the effective charge is  $\alpha = A/zl_B$ , where  $z$  is the largest valency; i.e., only counterions with the largest valency (here divalent ones) condense along the DNA, and no monovalent ions are condensed (unless divalent counterions are depleted, which is not the case in most of the experiments and especially not in ours).<sup>44</sup>

The OSF equation, eq 7, has thus been modified according to<sup>45,46</sup>

$$L_p^{\text{OSFM}} = L_p^0 + \frac{1}{4z^2 l_B \kappa^2} \quad (11)$$

which changes the slope  $B$  of the linear relationship  $L_p = L_p^0 + B/I$  from 0.559 (eq 9) to 0.033 nm·mol/L, and should be valid at low ionic strength, i.e., for large  $I^{-1}$ . This is the reason why the constant  $L_p^0$  is *a priori* different from that in eq 7,  $L_p^\infty$ . Note that adopting the Manning condensation, valid at low  $I$ , to the OSF calculation of the persistence length, valid at high  $I$ , is somewhat inconsistent. Moreover, eq 11 is not a proper asymptotic expansion in the limit  $\kappa A \rightarrow 0$ , since it leads to a diverging  $L_p$ . Of course, this limit cannot be reached in practice, since DNA counterions and ions resulting from water dissociation are always present even when no salt is added, which ensures that  $I \neq 0$  (even if it can be very small). Theoretically, the salt-free case corresponds to  $\kappa^{-1} \gg L$ , i.e., to ionic strengths  $I \ll 10^{-6} \text{ mol/L}$ , which is far from being the case in our experiments.

We fitted eq 11 to our experimental  $L_p$  values at low salt for the  $\text{Na}^+$  case, keeping  $L_p^0$  as a free parameter. The results, shown in Figure 5 (solid lines), are quite satisfactory, with  $L_p^0 = 51.3 \text{ nm}$  for  $L = 2060 \text{ bp}$  and  $48.8 \text{ nm}$  for  $L = 1201 \text{ bp}$  (keeping  $B$  free leads to a slightly higher value of  $B = 0.038 \text{ nm}\cdot\text{mol/L}$ ). However, eq 11 does not fit the  $L_p$  values for the  $\text{Mg}^{2+}$  case, the slope being larger (we found  $B \approx 0.1 \text{ nm}\cdot\text{mol/L}$ ), whereas eq 11 predicts a slope divided by  $z^2 = 4$ ,  $B = 0.008 \text{ nm}\cdot\text{mol/L}$ .

The persistence lengths measured in refs 5–7 and 47, at low  $I$  with  $\text{Na}^+$  ions, were fitted by  $L_p = L_p^0 + B/I$ . In ref 7,  $B = 0.033 \text{ nm}\cdot\text{mol/L}$  was fixed to the Manning value, and  $L_p^0$  was found to be around 45–50 nm. However, as already observed and discussed by Manning,<sup>15</sup> the fit is poor, and the error bars are quite large for low  $I$ . We checked that a parameter value of  $B =$

0.089 nm·mol/L, which does not correspond to any theoretical value, leads to a better fit (not shown). Maret et al.<sup>6</sup> fixed  $L_p^0 = 50$  nm and obtained reasonable fits with  $0.024 < B < 0.041$  nm·mol/L, which suggests a large error bar on the experimental values. Rizzo et al.<sup>5</sup> also fitted their data for  $3 < I < 1000$  mmol/L. They obtained  $L_p^0 = 46 \pm 1$  nm, in agreement with our value (see Figure 5), and  $B = 0.043$  nm·mol/L. Wenner et al.<sup>47</sup> measured  $L_p$  of dsDNA for various  $\text{Na}^+$  concentrations by fitting force–extension curves at low forces. They obtained  $L_p^0 = 46$  nm and  $B = 0.037$  nm·mol/L. All these values of  $B$  are in agreement with ours and the value predicted by eq 11, 0.033 nm·mol/L.

Tomić et al.<sup>48</sup> did dielectric spectroscopy experiments on semidilute DNA solutions with NaCl to investigate the high-frequency and low-frequency relaxation modes vs added salt concentration strength. In the high added salt limit (and relatively low DNA concentration), the length scale of the low-frequency relaxation mode,  $L_{LF}$ , can be interpreted as the DNA persistence length  $L_p$ . Their results are in qualitative agreement with the OSF–Manning theory, but with a coefficient  $B = 0.08$  nm·mol/L larger than the Manning value and smaller than the OSF value. Note that this discrepancy can be due to the fact that, in these experiments, the total ionic strength is different from the added salt concentration. Using the same experimental method, Tomić et al. investigated the effect of  $\text{Mg}^{2+}$  in solution.<sup>49</sup> The  $L_{LF}$  was about 1.5 times shorter in Mg–DNA solution than in Na–DNA solution, also suggesting an increased screening with  $\text{Mg}^{2+}$ . The behavior of  $L_{LF}$  was again explained by the OSF–Manning theory, but with a different value of the effective linear density.

Later, Manning proposed to modify eq 11 by multiplying the salt-dependent persistence length by a factor  $(2u - 1)/u \simeq 1.76$  for  $z = 1$  and 1.88 for  $z = 2$ , which gives a worse result for  $\text{Na}^+$  and is not sufficient for  $\text{Mg}^{2+}$  in our case.<sup>50</sup> This correction is therefore not suitable.

**5.3. Mean-Field Nonlinear Corrections at Intermediate Ionic Strengths.** In any case, eq 11 does not explain the concave shape shown in Figure 7 at intermediate ionic strengths. To do so requires renormalization factor for the DNA charge,  $\alpha$ , which depends on the ionic strength  $I$ . Such an approach was developed by Netz and Orland,<sup>51</sup> in which the Poisson–Boltzmann equation is variationally approximated by a Debye–Hückel equation with  $\alpha$  as a variational parameter which renormalizes the electrostatic potential at the DNA surface.

Here, we do the calculations by assuming that the DNA is not penetrable by ions, contrary to ref 51. The dimensionless electrostatic Debye–Hückel potential,  $\phi = ze\beta\psi$ , for an electrolyte (valency  $z$ ) of Debye–Hückel constant  $\kappa$  around a cylinder of radius  $R$  and surface charge density  $\sigma = 1/2\pi AR$  empty of ions is

$$\phi(r) = \frac{2u}{\kappa R} \frac{K_0(\kappa r)}{K_1(\kappa R)} \quad \text{for } r > R \quad (12)$$

$$\phi(r) = \frac{2u}{\kappa R} \frac{K_0(\kappa R)}{K_1(\kappa R)} \quad \text{for } r \leq R \quad (13)$$

where  $K_0$  and  $K_1$  are the modified Bessel function of order 0 and 1 and  $u = z l_B / A$  is the Manning parameter.

Following Netz and Orland,<sup>51</sup> the full nonlinear Poisson–Boltzmann equation is solved variationally by assuming that the solution is of the Debye–Hückel form,  $\alpha\phi(r)$ , where  $\phi(r)$  is

given in eq 12, and  $\alpha$ , the fraction of the “free” counterions, is the variational parameter and is the solution of (see the Supporting Information) the following:

$$4\pi z l_B (1 - \alpha) \int d\mathbf{r} \rho(\mathbf{r}) \phi(\mathbf{r}) = \kappa^2 \int d\mathbf{r} \Omega(\mathbf{r}) \phi(\mathbf{r}) \{ \sinh[\alpha\phi(\mathbf{r})] - \alpha\phi(\mathbf{r}) \} \quad (14)$$

where  $\rho(\mathbf{r}) = \sigma\delta(r - R)$  is the charge distribution. Note that the ionic exclusion factor  $\Omega(\mathbf{r})$  was incorrectly put just in front of the sinh in ref 51. Using eq 12, eq 14 simplifies to

$$2u(1 - \alpha)K_0(\kappa R) = \int_{\kappa R}^{\infty} x K_0(x) \left\{ \sinh \left[ \frac{2u\alpha}{\kappa R} \frac{K_0(x)}{K_1(\kappa R)} \right] - \frac{2u\alpha}{\kappa R} \frac{K_0(x)}{K_1(\kappa R)} \right\} dx \quad (15)$$

The solution  $\alpha(\kappa R)$ , where  $R \simeq 1$  nm is the DNA radius, is plotted in Figure 6 for  $z = 1$  (red) and  $z = 2$  (blue). The

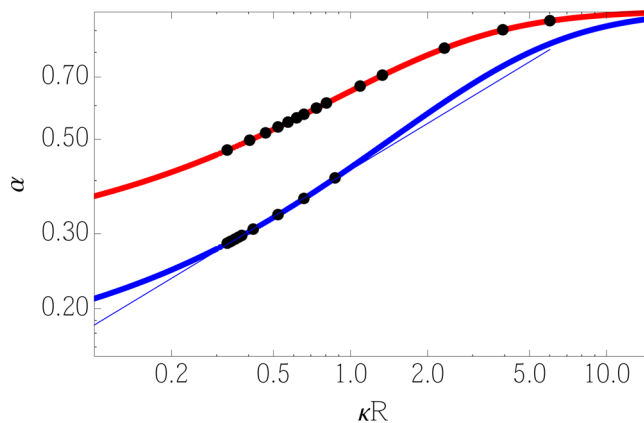


**Figure 6.** Renormalization charge parameter  $\alpha$  vs dimensionless screening parameter  $\kappa R$ , solution of eq 15 for  $u = 4.11$  (monovalent counterions in red) and  $u = 8.23$  (divalent counterions in blue). The black circles correspond to the experimental values studied in section 3.

renormalization factor  $\alpha$  is a monotonous increasing function of  $\kappa R$ , with  $\alpha(\kappa R \rightarrow \infty) \rightarrow 1$  and  $\alpha(\kappa R \rightarrow 0) \rightarrow 1/u$ . Hence it induces a concave shape to  $L_p$ , defined as

$$L_p^{\text{MF}} = L_p^0 + \frac{l_B}{4A^2\kappa^2} [\alpha(\kappa R)]^2 \quad (16)$$

One observes in Figure 6 that the variations of  $\alpha(\kappa R)$  are greater for  $z = 2$  than for  $z = 1$ . Moreover, for  $\kappa R \ll 1$ ,  $\alpha$  for  $z = 2$  is smaller than for  $z = 1$ . These two features are in qualitative agreement with what is observed in Figure 7.

To do a quantitative comparison of eq 16 with the experimental data in the whole range of ionic strengths, we used a polynomial interpolation function to fit  $L_p$  for monovalent ions ( $z = 1$ ), and a power law for divalent ions ( $z = 2$ ),  $\alpha(\kappa R) \simeq 0.423(\kappa R)^{0.364}$ , shown in Figure 6. The fitting parameters are  $L_p^0$  and a prefactor in front of the second term on the right-hand-side of eq 16 (expected to be close to 1). Fits are shown in Figure 7 as dashed lines. Clearly, this approach leads to a slightly concave curve for  $L_p(I^{-1})$  for the two types of counterions. However, whereas fits of  $\text{Mg}^{2+}$  data (in blue) are reasonably good ( $L_p^0 = 35.7$  nm, prefactor equal to 1.8 for  $L = 2060$  bp, and  $L_p^0 = 35.2$  nm, prefactor of 1.5 for  $L = 1201$  bp),

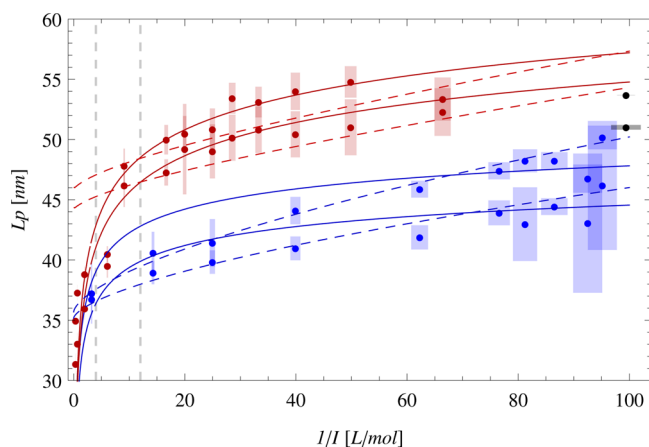


**Figure 7.** Same as Figure 5, where dashed lines are fits using eq 16 and solid lines using eq 19. Parameter values are given in the text.

the fits of the  $\text{Na}^+$  data are not good for  $I > 0.1$  mol/L ( $\Gamma^{-1} < 10$  L/mol), the concavity being not pronounced enough ( $L_p^0 = 44.2$  nm, prefactor of 0.8 for  $L = 2060$  bp, and  $L_p^0 = 45.9$  nm, prefactor of 0.9 for  $L = 1201$  bp). Moreover, here again the non-electrostatic contribution to the persistence length,  $L_p^0$ , varies from the fit of  $\text{Na}^+$  data to the fit of the  $\text{Mg}^{2+}$  data.

**5.4. Beyond Mean-Field: Ion–Ion Correlations and Thermal Fluctuations.** Other approaches have been proposed that go beyond the mean-field approximation by taking into account ion–ion correlations or/and thermal fluctuations.<sup>52–54</sup>

Nguyen et al.<sup>54</sup> considered ion–ion correlation in the strong coupling regime, defined as  $\Gamma = z^{3/2}l_B/(2RA)^{1/2} \gg 1$ . The theoretical limit  $\Gamma \rightarrow \infty$  corresponds to the freezing of the strongly coupled counterions into a Wigner crystal close to the DNA molecule. For  $\Gamma \gg 1$ , they found the following correction to the persistence length in the limit of zero ionic strength:

$$L_p = L_p^0 + \frac{R^2}{2zA}(-0.83\Gamma + 0.33\Gamma^{1/4} + 0.87) \quad (17)$$

which is independent of the ionic strength  $I$ . Therefore, they propose that  $L_p$  is constant at vanishing  $I$ . For DNA at room temperature, one has  $\Gamma = 1.2z^{3/2}$ , and applying eq 17 yields a correction of +0.65 nm for  $z = 1$  (even if  $\Gamma \approx 1$ ), and  $-2.20$  nm for  $z = 2$ . Equation 17 therefore qualitatively explains the observed abrupt decrease of  $L_p$  by about 5 nm when  $\text{Mg}^{2+}$  ions are added at very low  $I$  in the buffer: the monovalent  $\text{Na}^+$  ions are replaced by strongly coupled divalent counterions, whose correlations decrease the global free energy of the condensed ions and therefore the DNA bending free energy. Hence,  $L_p(I \rightarrow 0)$  decreases with  $z$ . Following this approach, it is thus consistent to choose two different asymptotic values for  $L_p$  when  $I \rightarrow 0$  for monovalent and divalent ions. This explains why these values were slightly different (by about 9 nm) in the preceding section. Note that this theory explains the constant shift at very low  $I$  but does not explain the change in the shape of  $L_p(\Gamma^{-1})$ .

Thermal fluctuations were taken into account by Golestanian et al.,<sup>53</sup> who obtained a correction to the persistence length due to fluctuation-induced correlations between ions. Indeed, they correct the OSF–Manning formula, eq 11, at low  $\kappa A$ , following

$$L_p = L_p^0 + \frac{l_B}{4u^2(\kappa A)^2}f(\kappa A, u) \quad (18)$$

where  $f(\kappa A, u) = [1 - 2(u - 1) \ln(\kappa A)]^{-2}$ . Ariel and Andelman<sup>52</sup> proposed a similar correction, with  $f(\kappa A, u) = u(2 - u) - (u - 1)^2/[u \ln(\kappa A)]$ .

Both formulas do not apply to DNA for  $z = 1$  and 2 ( $u = 4.21$  and 8.41). Golestanian's formula yields a slope that is divided by almost 200, with a convex shape for  $\Gamma^{-1} < 10$  L/mol, and Ariel's formula yields a decreasing function of  $L_p(\Gamma^{-1})$  as  $\Gamma^{-1}$  increases for the whole  $I$  range. These two theories are therefore not consistent with the whole set of experimental data shown in section 3.

**5.5. Manning's Internal Stretching Force Calculation for  $L_p$ .** The major issue in trying to fit the above theories for the whole range of ionic strengths is to find a fit that yields the concave shape observed for the experimental values. Equation 7, *a priori* valid for high  $I$ , and eq 11, valid for low  $I$ , cannot be reconciled because the constant value is clearly different in both cases,  $L_p^0 > L_p^\infty$ , and should therefore vary with  $I$ .

Manning noted this discrepancy in 2006,<sup>15</sup> and proposed a new formula for the persistence length taking into account the internal electrostatic tension due to the repulsion between charges along the polyelectrolyte. He adapted the calculation reported by Netz<sup>55</sup> for strongly stretched polyelectrolytes at the Debye–Hückel level to the framework of the counterion condensation approach to obtain the persistence length of a polyelectrolyte as a function of  $\kappa A$  and the persistence length of the so-called null isomer (the hypothetical structure of the polyelectrolyte if the backbone charges are set to zero),  $L_p^*$ :

$$L_p = \left(\frac{\pi}{2}L_p^*\right)^{2/3} \frac{R^{4/3}}{z^2l_B} \left[ (2u - 1) \frac{\kappa A e^{-\kappa A}}{1 - e^{-\kappa A}} - 1 - \ln(1 - e^{-\kappa A}) \right] \quad (19)$$

Equation 19 fits very well our data for the  $\text{Na}^+$  case over the whole ionic range with only one fitting parameter,  $L_p^*$  (Figure 7). The fitting values are  $L_p^* = 6.0$  nm (for  $L = 2060$  bp) and 5.4 nm (for  $L = 1201$  bp), close to the value of 7.4 nm fitted by Manning using various experimental data for long DNA ( $L \approx 40$  kbp).<sup>15</sup> This suggests the phenomenological scaling  $L_p^*(L) \approx 3.07L^{0.083}$ .

Savelyev<sup>4</sup> performed numerical simulations to investigate the dependence of the persistence length of double-stranded DNA on solutions with various ionic strengths. A coarse-grained model of a two-bead DNA chain with explicit mobile ions ( $\text{Na}^+$  and  $\text{Cl}^-$  ions)<sup>16</sup> was designed to reproduce physical salt conditions from  $10^{-4}$  to 0.1 mol/L (the water solvent is implicit). Their numerical results for  $L_p(I)$  are in semi-quantitative agreement with eq 19 for  $I > 0.1$  mol/L. For lower  $I$ , the agreement is better with the OSF theory, eq 7 (see Figure 2 of ref 4; the fitting parameter values are not given). This was confirmed in other molecular dynamics simulations,<sup>56</sup> where the non-electrostatic contribution to  $L_p$  (with the DNA charges set to 0) appeared to be much larger than the  $L_p^*$  value found by Manning. Moreover, Savelyev<sup>4</sup> compared previous experimental results to his simulations and found a qualitative agreement.

Assuming that, according to the counterion condensation theory,<sup>44</sup> all the condensed counterions are divalent, we use the same formula for the persistence lengths with  $\text{Mg}^{2+}$  counterions. It leads to poorer fits (Figure 7) with very different values for  $L_p^*$ : 14.1 nm (for  $L = 2060$  bp) and 12.7 nm (for  $L = 1201$  bp). The fact that  $L_p^*$  varies, and increases, with the counterion

valency is puzzling. Hence, the dependence of  $L_p$  on  $z$  in eq 19 is not consistent with our experimental data.

## 6. INTERPOLATION FORMULA FOR THE WHOLE IONIC STRENGTH RANGE

We propose the following interpolation formula to fit the four sets of data (two DNA lengths, monovalent and divalent salts) over the whole  $I$  range:

$$L_p = L_p^\infty + \frac{L_p^0 - L_p^\infty}{1 + (I/I_0)^\delta} \quad (20)$$

with four fitting parameters:  $L_p^0$ ,  $L_p^\infty$ ,  $I_0$ , and  $\delta$ . The fits, shown in Figure 8, are very good for the monovalent  $\text{Na}^+$  ion, with  $L_p^0 =$

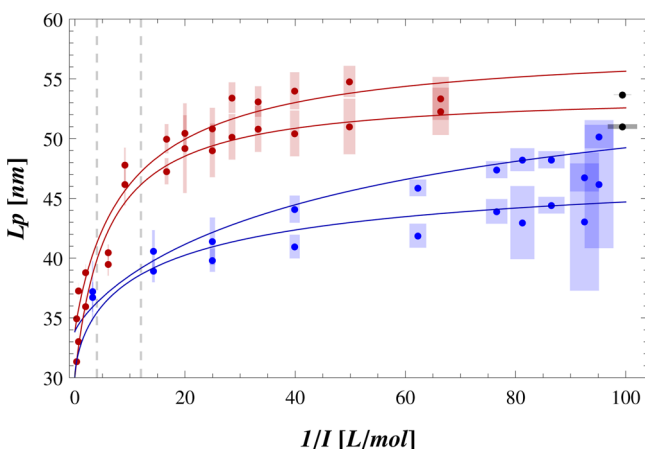


**Figure 8.** DNA persistence length,  $L_p$ , vs the inverse of the ionic strength,  $I^{-1}$ , extracted from the HT-TPM data. The red (resp. blue) symbols correspond to buffers with sodium (resp. magnesium) counterions (top curves are for  $L = 2060$  bp and bottom curves for  $L = 1201$  bp). The solid lines are fits using eq 20 with parameter values given in the text.

58.1 nm,  $L_p^\infty = 33.8$  nm,  $I_0 = 0.104$  mol/L, and  $\delta = 0.931$  for  $L = 2060$  bp, and  $L_p^0 = 53.9$  nm,  $L_p^\infty = 30.1$  nm,  $I_0 = 0.174$  mol/L, and  $\delta = 0.994$  for  $L = 1201$  bp.

Several comments are in order. First, as expected, the asymptotic values,  $L_p^\infty$  and  $L_p^0$ , are, at about 2 nm, the same as those extracted from the linear OSF and OSF–Manning fits shown in Figure 5. Next, the value of the crossover ionic strength,  $I_0$ , is on the order of 0.1 mol/L, which corresponds to a Debye screening length  $\kappa_0^{-1} \approx 1$  nm, i.e., on the order of the DNA radius,  $R$ . There thus suggest that the concave shape, which is more pronounced for  $I \approx I_0$ , comes from nonlinear Poisson–Boltzmann effects, as illustrated in section 5.3. Moreover, the effective power law for  $I \approx I_0$  is found by doing a logarithmic expansion of eq 20 around  $I_0$ :

$$\ln(L_p - L_p^\infty) \approx \ln\left(\frac{L_p^0 - L_p^\infty}{2}\right) - \frac{\delta}{2} \ln\left(\frac{I}{I_0}\right) \quad (21)$$

which yields an exponent  $-\delta/2 \approx 0.5$ , which is a good approximation for  $0.05 < I < 0.5$  mol/L (error less than 1 nm). Finally, at low ionic strength,  $I \ll I_0$ , eq 20 varies slightly, and the curve looks like a linear law as a function of  $I^{-1}$  with a small slope, as suggested by eq 11. At large ionic strength,  $I \gg I_0$ , eq 20 yields  $L_p \approx L_p^\infty + (L_p^0 - L_p^\infty)(I_0/I)^\delta$ , which is equivalent to eq 7 for  $\delta = 1$ , but with a slightly larger slope of 2–4 nm·L/mol.

For divalent  $\text{Mg}^{2+}$  ions, the fits are also good, but with different values for  $\delta$  and  $I_0$  as compared to the  $\text{Na}^+$ -only case. The parameter values  $L_p^\infty$  are equal to those in the  $\text{Na}^+$  case, and the values of  $L_p^0$  are comparable:  $L_p^0 = 59.2$  nm,  $I_0 = 0.017$  mol/L, and  $\delta = 0.830$  for  $L = 2060$  bp, and  $L_p^0 = 51.7$  nm,  $I_0 = 0.045$  mol/L, and  $\delta = 0.546$  for  $L = 1201$  bp. As expected, the concavity is less pronounced and shifted to lower values of  $I$ , close to  $I_0$ . Thus, eq 20 can be useful for experimentalists to interpolate values of  $L_p$  over the whole range of  $I$ .

## 7. CONCLUSION

**7.1. Summary.** Using the high-throughput tethered particle motion setup, we measured the impact of the ionic strength on DNA conformation for two DNA samples of lengths 2060 and 1201 bp. To this end, we investigated a large and homogeneously distributed range of ionic strengths,  $I \in [0.01, 3]$  mol/L, by adding salt to the buffer with monovalent  $\text{Na}^+$  or divalent  $\text{Mg}^{2+}$  counterions. Experimental drift and biases due to the finite exposure time of the detector were corrected. To extract properly the DNA persistence length,  $L_p$ , from the HT-TPM amplitude of motion,  $R_{\text{exp}}$ , numerical exact sampling simulations (without explicit mobile ions and solvent) were performed. Both the DNA excluded volume and that of the particle were taken into account. These simulations allowed us to obtain the experimental  $L_p$  as a function of  $I$  with a good accuracy of about 4% (Figure 7). When  $L_p$  is plotted as a function of  $I^{-1}$ , the overall trend is a monotonous increasing function with, for the  $\text{Na}^+$  case, a concave shape, and, for the  $\text{Mg}^{2+}$  one, an almost linear shape (except at very low concentrations of  $\text{Mg}^{2+}$ ).

Our results are compared to other results found in the literature. A quantitative comparison is difficult, since the  $L_p$  values fluctuate appreciably depending on the experimental setup and the method of extraction of  $L_p$ . Hence, for instance at  $I \approx 150$  mmol/L,  $L_p$  lies between 40 and 74 nm (Table 1). The available experimental values can, as proposed by Savelyev et al.,<sup>4</sup> be divided into two sets of data. The global behavior of our measured  $L_p$  with  $I$  is not coherent with the first set nor with the second set of experiments. On one hand, our  $L_p$  values appear to be in agreement with the slow increase (of 10%) of  $L_p$  observed by the first group at low  $I$ . On the other hand, at high  $I$ , our  $L_p$  values show a significant 25% variation, in perfect agreement with the experiments of the second group.

Our experimental  $L_p$  values follow a linear OSF law in  $I^{-1}$  only for a very small range of ionic strengths at high  $I$ , with a different prefactor than predicted by OSF in eq 7.

For monovalent  $\text{Na}^+$  counterions,  $L_p$  varies linearly with  $I^{-1}$  at very low  $I$ , according to the OSF equation using the Manning counterion condensation theory, eq 11. The whole  $I$  range is furthermore well fitted by eq 19, which takes into account both the DNA internal stretching due to phosphate ions of the backbone and the counterion condensation around the DNA.

For divalent  $\text{Mg}^{2+}$  counterions, however, neither eq 11 nor eq 19 (with the same fitting parameter as for  $\text{Na}^+$ ) fits well the data. This suggests that these theories do not reproduce well the observed dependence on the valency  $z$ . Using a variational approach taking into account both nonlinear Poisson–Boltzmann effects and screening by mobile ions, we propose a reasonable fit for both the  $\text{Na}^+$  and the  $\text{Mg}^{2+}$  cases, but only for  $I < 0.1$  mol/L and with two different values of  $L_p^0$  at vanishing ionic strength. This marked decrease of  $L_p^0$  at very low  $I$ , when a very small amount of  $\text{Mg}^{2+}$  ions is added, is

semiquantitatively explained by a theory that considers ion–ion correlations, eq 17, for large  $z$ .

In order to both interpolate  $L_p$  values between the ones effectively measured and compare with future experimental data, we proposed an empirical formula that fits both the monovalent and divalent cases.

**7.2. Concluding Remarks.** The large scattering of the available experimental  $L_p$  values observed in Figure 4 may be due to the different experimental setups but also to the various buffers used in these experiments. Indeed, we have shown that the presence of traces of divalent ions, which are often present in buffers in order to maintain the fixed pH, can substantially decrease the  $L_p$  value at a given ionic strength.

An illustration of the extreme sensitivity of persistence length values to the experimental method and the model employed to extract the results was shown by Mielke et al.<sup>57</sup> Brownian dynamics simulations on a double-stranded DNA in a bulk environment were performed at different salt concentrations. Two different strategies were employed to calculate  $L_p$  from the simulation results. One used the expression of the WLC model, eq 1, and the other used an approximation proposed by Hagerman<sup>2</sup> for the rotational diffusion coefficients in order to directly connect to the experimental results of ref 27. At low concentrations, depending on the method used,  $L_p(I)$  shows two distinct behaviors. Values from the rotational diffusion coefficients were more than 30 times larger than the WLC values and Hagerman's values. This result highlights the effects of the chosen model to extract  $L_p$  and the rough approximation used in earlier models to extract it from DLS measurements.

Furthermore, it was recently shown that HT-TPM can detect the effect of the DNA sequence, in particular the presence of A-tracts, on the DNA conformation, which has been interpreted as a modification of the DNA's spontaneous curvature.<sup>19</sup> Preliminary results also show that, for a given DNA length but two different sequences, the persistence length varies. It is thus tempting to suggest that the bare, non-electrostatic contribution to  $L_p$  can also be sequence-dependent, and this can be another explanation for the data scattering.

Finally, many experiments study the influence of ions with higher valency—for instance, trivalent ions such as spermidine, which also has a strong effect on  $L_p$  at millimolar concentrations<sup>7,36</sup>—and/or the role of multivalent ions on the DNA melting temperature.<sup>58</sup> It would be interesting to pursue such a quantitative study of the DNA conformation for such trivalent ions, and thus to study the interplay between screening effects, condensation,<sup>59</sup> and denaturation.<sup>60</sup>

On the theoretical side, a complete theory that explains the variations of  $L_p$  as a function of both  $I$  and the counterion valency  $z$  is still lacking. The approach used by Manning<sup>15</sup> is appealing since it fits very well the experimental data for monovalent counterions with only one fitting parameter. However, the precise treatment of ion–ion correlations should be taken into account to extend such a theory to counterions with higher valencies. Note that these approaches do not consider dielectric exclusion close to a low dielectric molecule such as DNA<sup>61,62</sup> or van der Waals interactions, which are also modified when the ionic strength is varied.

In this paper, we assumed that, according to the WLC model, the tangent–tangent correlation function is a simple exponential, eq 1, which therefore leads to a single correlation length,  $L_p$ . However, Barrat and Joanny show that, by taking into account the polymer bending fluctuations, the persistence length is scale-dependent.<sup>63</sup> A more appropriate choice would

be a double exponential where  $\langle \mathbf{t}(s) \cdot \mathbf{t}(0) \rangle \simeq 1 - s/L_p^\infty$  at small length scales and  $\langle \mathbf{t}(s) \cdot \mathbf{t}(0) \rangle = \exp(-s/L_p^{\text{OSF}})$  at large length scales, where the crossover depends on the ionic strength. It has been shown<sup>64</sup> that  $L_p^{\text{OSF}}$  is given by eq 7 and  $L_p^\infty$  is the bare persistence length. Another approach proposed that the latter is also salt-dependent.<sup>65</sup> Of course, such a model is more difficult to apply to the experimental measure of  $R_{\text{DNA}}$  only, with a rather tricky extraction of two different correlation lengths, but it might provide a relevant framework to explain the overall observed behaviors of  $L_p(I)$ .

## ■ ASSOCIATED CONTENT

### 📄 Supporting Information

Plots of DNA approximate end-to-end distances, tables of experimental data, and theoretical complements. The Supporting Information is available free of charge on the ACS Publications website at DOI: 10.1021/acs.macromol.5b00735.

## ■ AUTHOR INFORMATION

### ✉ Corresponding Author

\*E-mail: manghi@irsamc.ups-tlse.fr.

### 📝 Notes

The authors declare no competing financial interest.

## ■ ACKNOWLEDGMENTS

We thank Oriol Servera Sires for his valuable B.Sc. work on the fitting procedure, and Juliette Wilhem who helped with the experiments as part of her Master's project. We acknowledge financial support from the CNRS, University of Toulouse 3, and ANR-11-NANO-010 TPM-On-a-Chip.

## ■ REFERENCES

- (1) Harrington, R. E. *Biopolymers* **1978**, *17*, 919.
- (2) Hagerman, P. J. *Biopolymers* **1981**, *20*, 1503.
- (3) Borochoy, N.; Eisenberg, H.; Kam, Z. *Biopolymers* **1981**, *20*, 231.
- (4) Savelyev, A. *Phys. Chem. Chem. Phys.* **2012**, *14*, 2250.
- (5) Rizzo, V.; Schellmann, J. *Biopolymers* **1981**, *20*, 2143.
- (6) Maret, G.; Weill, G. *Biopolymers* **1983**, *22*, 2727.
- (7) Baumann, C. G.; Smith, S. B.; Bloomfield, V. A.; Bustamante, C. *Proc. Natl. Acad. Sci. U.S.A.* **1997**, *94*, 6185.
- (8) Manning, G. S. *Biopolymers* **1981**, *20*, 1751.
- (9) Kam, Z.; Borochoy, N.; Eisenberg, H. *Biopolymers* **1981**, *20*, 2671.
- (10) Cairney, K. L.; Harrington, R. E. *Biopolymers* **1982**, *21*, 923.
- (11) Post, C. B. *Biopolymers* **1983**, *22*, 1087.
- (12) Sobel, E. S.; Harpst, J. A. *Biopolymers* **1991**, *31*, 1559.
- (13) Odijk, T. J. *Polym. Sci.* **1977**, *15*, 477.
- (14) Skolnick, J.; Fixman, M. *Macromolecules* **1977**, *10*, 944.
- (15) Manning, G. S. *Biophys. J.* **2006**, *91*, 3607.
- (16) Savelyev, A.; Papoian, G. A. *Proc. Natl. Acad. Sci. U.S.A.* **2010**, *107*, 171.
- (17) Peters, J. P.; Maher, L. J., III. *Q. Rev. Biophys.* **2010**, *43*, 23.
- (18) Plenat, T.; Tardin, C.; Rousseau, P.; Salomé, L. *Nucleic Acids Res.* **2012**, *40*, e89.
- (19) Brunet, A.; Chevalier, S.; Destainville, N.; Manghi, M.; Rousseau, P.; Salhi, M.; Salomé, L.; Tardin, C. *Nucleic Acids Res.* **2015**, DOI: 10.1093/nar/gkv201.
- (20) Pouget, N.; Dennis, C.; Turlan, C.; Grigoriev, M.; Chandler, M.; Salomé, L. *Nucleic Acids Res.* **2004**, *32*, e73.
- (21) Manghi, M.; Tardin, C.; Baglio, J.; Rousseau, P.; Salomé, L.; Destainville, N. *Phys. Biol.* **2010**, *7*, 046003.
- (22) Destainville, N.; Salomé, L. *Biophys. J.* **2006**, *90*, L17.
- (23) Segall, D. E.; Nelson, P.; Phillips, R. *Phys. Rev. Lett.* **2006**, *96*, 4.
- (24) Doi, M.; Edwards, S. F. *The Theory of Polymer Dynamics*; Oxford University Press: Oxford, 1986.

- (25) Yamakawa, H. *Helical Wormlike Chains in Polymer Solutions*; Springer-Verlag: Berlin, 1997.
- (26) Palmeri, J.; Manghi, M.; Destainville, N. *Phys. Rev. E* **2008**, *77*, 011913.
- (27) Hagerman, P. J. *Ann. Rev. Biophys. Biophys. Chem.* **1988**, *17*, 265.
- (28) Porschke, D. *Biophys. Chem.* **1991**, *40*, 169.
- (29) Elias, J. G.; Eden, D. *Macromolecules* **1981**, *14*, 410.
- (30) Elias, J. G.; Eden, D. *Biopolymers* **1981**, *20*, 2369.
- (31) Diekmann, S.; Hillen, W.; Morgeneyer, B.; Wells, R. D.; Porschke, D. *Biophys. Chem.* **1982**, *15*, 263.
- (32) Porschke, D. *J. Biomol. Struct. Dyn.* **1986**, *4*, 373.
- (33) Bednar, J.; Furrer, P.; Katritch, V.; Stasiak, A.; Dubochet, J.; Stasiak, A. *J. Mol. Biol.* **1995**, *254*, 579.
- (34) Lu, Y.; Weers, B.; Stellwagen, N. C. *Biopolymers* **2002**, *61*, 261.
- (35) Borochoy, N.; Eisenberg, H. *Biopolymers* **1983**, *23*, 1757.
- (36) Wang, M. D.; Yin, H.; Landick, R.; Gelles, J.; Block, S. M. *Biophys. J.* **1997**, *72*, 1335.
- (37) Mantelli, S.; Muller, P.; Harlepp, S.; Maaloum, M. *Soft Matter* **2011**, *7*, 3412.
- (38) Smith, S. B.; Finzi, L.; Bustamante, C. *Science* **1992**, *258*, 1122.
- (39) Dietrich, H. R. C.; Rieger, B.; Wiertz, F. G. M.; De Groote, F. H.; Heering, H. A.; Young, I. T.; Garini, Y. *J. Nanophoton.* **2009**, *3*, 031795.
- (40) Han, L.; Lui, B. H.; Phillips, R. In *Mathematics of DNA Structure, Function and Interactions*; Benham, C., Harvey, J. S., Olson, W. K., Summers, D. W. L., Swigon, D., Eds.; Springer: New York, 2009; pp 123–138.
- (41) Kumar, S.; Manzo, C.; Zurla, C.; Ucuncuoglu, S.; Finzi, L.; Dunlap, D. *Biophys. J.* **2014**, *106*, 399.
- (42) Fixman, M. *J. Phys. Chem. B* **2010**, *114*, 3185.
- (43) Manning, G. S. *J. Chem. Phys.* **1969**, *51*, 924.
- (44) Manning, G. S. *J. Chem. Phys.* **1984**, *88*, 6654.
- (45) Le Bret, M. *J. Phys. Chem.* **1982**, *76*, 6243.
- (46) Fixman, M. *J. Phys. Chem.* **1982**, *76*, 6346.
- (47) Wenner, J. R.; Williams, M. C.; Rouzina, I.; Bloomfield, V. A. *Biophys. J.* **2002**, *82*, 3160.
- (48) Tomić, S.; Vuletić, T.; Dolanski Babić, S.; Krča, S.; Ivanković, D.; Griparić, L.; Podgornik, R. *Phys. Rev. Lett.* **2006**, *97*, 098303.
- (49) Grgičin, D.; Dolanski Babić, S.; Ivek, T.; Tomić, S.; Podgornik, R. *Phys. Rev. E* **2013**, *88*, 052703.
- (50) Manning, G. S. *Macromolecules* **2001**, *34*, 4650.
- (51) Netz, R. R.; Orland, H. *Eur. Phys. J. E* **2003**, *11*, 301.
- (52) Ariel, G.; Andelman, D. *EPL* **2003**, *61*, 67.
- (53) Golestanian, R.; Kardar, M.; Liverpool, T. *Phys. Rev. Lett.* **1999**, *82*, 4456.
- (54) Nguyen, T. T.; Rouzina, I.; Shklovskii, B. *Phys. Rev. E* **1999**, *60*, 7032.
- (55) Netz, R. R. *Macromolecules* **2001**, *34*, 7522.
- (56) Savelyev, A.; Materese, C. K.; Papoian, G. A. *J. Am. Chem. Soc.* **2011**, *133*, 19290.
- (57) Mielke, S. P.; Benham, C. J.; Grønbech-Jensen, N. *J. Phys. Chem. A* **2009**, *113*, 4213.
- (58) Owczarzy, R.; Moreira, B. G.; You, Y.; Behlke, M. A.; Walder, J. A. *Biochemistry* **2008**, *47*, 5336.
- (59) Bloomfield, V. A. *Curr. Opin. Struct. Biol.* **1996**, *6*, 334.
- (60) Korolev, N.; Lyubartsev, A. P.; Nordenskiöld, L. *Biophys. J.* **1998**, *75*, 3041.
- (61) Chertsvy, A. G. *J. Phys. Chem. B* **2007**, *111*, 12933.
- (62) Buyukdagli, S.; Manghi, M.; Palmeri, J. *Phys. Rev. E* **2010**, *81*, 041601.
- (63) Barrat, J.-L.; Joanny, J.-F. *Europhys. Lett.* **1993**, *24*, 333.
- (64) Manghi, M.; Netz, R. R. *Eur. Phys. J. E* **2004**, *14*, 67.
- (65) Gubarev, A.; Carrillo, J.-M. Y.; Dobrynin, A. V. *Macromolecules* **2009**, *42*, 5851.
- (66) Ramanathan, G. V. *J. Chem. Phys.* **1983**, *78*, 3223.
- (67) Stellwagen, N. C. *Biopolymers* **1981**, *20*, 399.